

Microscopic characterization of defect structure in RDX crystals

R. H. B. BOUMA*, W. DUVALOIS† & A. E. D. M. VAN DER HEIJDEN†, ‡

*TNO, Research Group Gas Treatment, NL-2600 JA Delft, the Netherlands

†TNO, Research Group Energetic Materials, NL-2280 AA Rijswijk, the Netherlands

‡Department Process & Energy, Section Intensified Reaction and Separation Systems, Delft University of Technology, Stevinweg 1, 2628 CN Delft, the Netherlands

Key words. Confocal scanning laser microscopy, crystal defects, crystal growth, electron microscopy, explosives, RDX.

Summary

Three batches of the commercial energetic material RDX, as received from various production locations and differing in sensitivity towards shock initiation, have been characterized with different microscopic techniques in order to visualize the defect content in these crystals. The RDX crystals are embedded in an epoxy matrix and cross-sectioned. By a treatment of grinding and polishing of the crystals, the internal defect structure of a multitude of energetic crystals can be visualized using optical microscopy, scanning electron microscopy and confocal scanning laser microscopy. Earlier optical micrographs of the same crystals immersed in a refractive index matched liquid could visualize internal defects, only not in the required detail. The combination of different microscopic techniques allows for a better characterization of the internal defects, down to inclusions of approximately $0.5\ \mu\text{m}$ in size. The defect structure can be correlated to the sensitivity towards a high-amplitude shock wave of the RDX crystals embedded in a polymer bonded explosive. The obtained experimental results comprise details on the size, type and quantity of the defects. These details should provide modellers with relevant and realistic information for modelling defects in energetic materials and their effect on the initiation and propagation of shock waves in PBX formulations.

Introduction

The crystallization of a substance is subject to increasingly stringent demands regarding, for example, its purity, particle shape, particle size distribution, stability and shelf-life (Van der Heijden & Ter Horst, 2005). The crystallization conditions (growth kinetics, hydrodynamics, hardware geometry, scale of operation, etc.) under which these substances are produced, as well as the processing solvents used, influence

these properties. Improvement of current production techniques and the design of new processes therefore focus on how these product demands can be fulfilled in an economically feasible way.

Energetic materials, such as oxidizers and explosives, are generally based on CHNO-containing molecules. The presence of oxygen (in excess in case of oxidizers) and nitrogen in these energetic molecules leads to the formation of large amounts of relatively small, gaseous molecules during decomposition or combustion of the energetic material. These gases can be used to propel a rocket or sustain a detonation. In these types of energetic compositions (propellants and secondary explosives), the energetic particles are mixed with a polymer at solid loads up to 80–85 wt% that, after casting, is chemically cured to obtain a composition consisting of energetic materials embedded in a rubbery matrix, forming a solid composite propellant, in case of oxidizers, or a polymer bonded explosive (PBX) in case of explosive particles.

Energetic materials form a special class of substances that generally require additional demands with respect to their hazardous properties: sensitiveness to friction and impact stimuli, thermal instabilities and incompatibilities with other ingredients may lead to undesired initiation of these energetic materials, posing a potential risk to military personnel, material and infrastructure. In particular, for shock stimuli, it was shown that the presence of defects in energetic crystals, like dislocations and inclusions, determines the shock pressure that is needed to initiate an explosive: generally it can be stated that an explosive is more easy to initiate if the energetic crystals have a poor quality (high-defect content). Only a relatively small increase in HMX crystal density from 1.886 to $1.902\ \text{g cm}^{-3}$ almost doubled the shock initiation pressure of these crystals when immersed in a liquid or dispersed in a polymeric matrix, demonstrating the significant gains to be made in vulnerability reduction (Kröber *et al.*, 1998; Van der Heijden & Bouma, 1998; Van der Heijden *et al.*, 2000). It is less clear, however, which types of defects (e.g. macro- or microinclusions) are responsible for determining the value of the shock

Correspondence to: R. H. B. Bouma, TNO, Research group Gas Treatment, PO Box 6012, NL-2600 JA Delft, the Netherlands. Tel: +31-888661420; e-mail: richard.bouma@tno.nl

initiation pressure. Therefore, the characterization of the defect content of energetic crystals has been the subject of many research studies (e.g. Borne, 1993; Van der Heijden & Bouma, 2004; Van der Heijden *et al.*, 2004; Van der Heijden & Bouma, 2010). In parallel, manufacturers attempted to improve their products, finally leading to the commercial introduction of several types of insensitive RDX (research developed explosive, cyclotrimethylene trinitramine, $C_3H_6N_6O_6$) by different companies in the past decade. The use of this reduced sensitivity RDX in explosive compositions has led to less shock sensitive munitions. These developments further contributed to the concept of insensitive munitions (IM), already introduced in the 1960s following severe accidents involving munitions (Beauregard, 2004), aiming at significant reductions of the risks of undesired munitions responses towards external threats (e.g. bullet or fragment impact, fire, shock, etc.).

In an international reduced-sensitivity RDX Round Robin program, RDX Class 1 crystals from seven different sources were distributed blind to participating laboratories (Watt *et al.*, 2006; Doherty & Watt, 2008). One of the aims of this Round Robin was to search for a measurable property of the RDX crystal quality with unequivocal relation to the shock sensitivity of an RDX-based explosive composition. The mandatory tests that were thought to be discriminating regarding crystal quality and shock sensitivity, comprised optical microscopy of crystals in a contrasting or refractive index matched liquid, scanning electron microscopy (SEM) of crystals, crystal density distribution determination via a flotation method and gas or liquid pycnometry for determining the average crystal density. However, no conclusive argument could be made regarding a measurable and crystal quality related property, and the shock sensitivity of a cast PBX. Additional research was carried out at the crystal level using line broadening in nuclear quadrupole resonance (Doherty *et al.*, 2006) and in X-ray diffraction (Förster-Barth *et al.*, 2007), a modified differential scanning calorimetric method (Spyckerelle, 2006; Spyckerelle *et al.*, 2010), SEM applied to cleaved crystal surfaces (Van der Heijden *et al.*, 2008; Van der Heijden & Bouma, 2010), impact testing with a ballistic impact chamber (Bouma *et al.*, 2008) and nanoindentation (Hudson *et al.*, 2013).

For completeness, it has to be understood that not only crystal defects contribute to the shock sensitivity of PBXs. Other contributors are, for example, the local propagation, focusing and divergence of the shock wave when crossing the polymer/energetic crystal interface (Baer, 2002; Handley, 2011), shape and mean size of the energetic crystals (Moulard, 1989; Qiu *et al.*, 2011) and incomplete wetting of the energetic crystals by the polymeric binder. In this paper, however, the focus is on the internal defect structure of the RDX crystals, being the main source determining the shock initiation pressure at the PBX level. The objective of this study was to visualize the internal defect structure of three RDX batches selected from the Round Robin program by means of optical microscopy, SEM and confocal scanning laser microscopy (CSLM) and to

Table 1. Sources of the RDX crystals, a quality assessment based on optical micrographs of crystals immersed in a refractive index matched liquid and shock initiation pressure of RDX crystals in composition PBXN-109 (Doherty & Watt, 2008), crystal density and impurity content, that is, HMX by HPLC, cyclohexanone and acetone by GC for two separate sample preparations (Watt *et al.*, 2006)

RDX	K1	K6	K7
Source	BAe Royal Ordnance	Dyno Type II	ADI
Quality	intermediate	bad	good
$P_{\text{initiation}}$ (kbar)	50.6	38.6	53.3
ρ_{crystal} ($g\ cm^{-3}$)	1.795	1.804	1.794
HMX (%)	0.19	8.55	0.02
Cyclohexanone (%)	0.72/0.87	0.00/0.01	0.58/0.69
Acetone (%)	0.00/0.049	0.045/0.068	0.045/0.085

correlate the defect structure with the sensitivity towards a high-amplitude shock wave of the RDX crystals embedded in a PBX, as has been assessed in the aforementioned Round Robin program.

Experiment

Three RDX qualities from the aforementioned Round Robin program have been selected for further study, based on (i) the shock initiation pressure of these RDX grades when embedded in the polymer-bonded explosive PBXN-109 consisting of 64 wt% RDX, 20 wt% aluminum and a 16 wt% hydroxyl-terminated polybutadiene binder system and (ii) a qualitative assessment (good, intermediate, bad) based on the optical micrographs of the RDX crystals immersed in a refractive index matched liquid. The samples are referred to as K1, K6 and K7. All samples contain large and distinguishable voids, although their number density may differ. Especially K6 and to a lesser extent K1 contain 'greyish' areas, which might be related to the presence of many small inclusions localized in a small volume in the crystal (Watt *et al.*, 2006; Van der Heijden *et al.*, 2008). The source of the RDX crystals, shock initiation pressure, crystal density and impurity content are reproduced in Table 1 (Watt *et al.*, 2006; Doherty & Watt, 2008). The HMX present in the samples is a by-product in one of the RDX synthesis processes. The presence of cyclohexanone and acetone are indicative of the solvents used in the crystallization processes.

Sample preparation

Samples are prepared by embedding the RDX crystals in an epoxy matrix in order to observe the internal defects in the RDX crystals. Samples have been obtained by taking a scoop while gently moving through the larger volume of each of the three different RDX batches. The epoxy matrix is prepared by

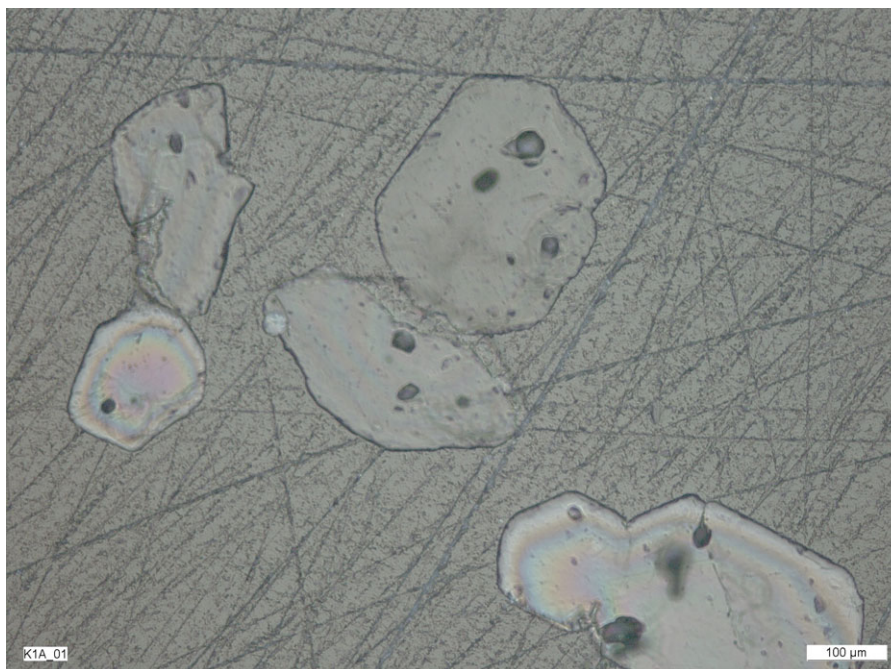


Fig. 1. Optical micrograph of K1 RDX crystals in incident light mode.

mixing a resin and hardener (EPO-THIN) from Buehler Ltd., in a 5:2 ratio by weight. The mixture is stirred for 2 min and transferred to a vacuum oven to let the evolved gases escape. The epoxy mixture is carefully poured into plastic cups with the RDX crystals covering the bottom surface. After curing the epoxy mixture over night at room temperature, the plastic cups are removed. The epoxy surface containing the RDX crystals is polished using a Motopol 8 polishing machine from Buehler Ltd. Sequential steps were planar grinding using SiC P1200 paper with water, polishing using a Nylon disc with first a 6- μm and then a 3- μm diamond particle oil suspension, and polishing with MasterTex® cloth using a colloidal silicon cloth (0.06 μm) fluid. In between polishing steps, the surface is cleaned from particles and fluids. A microscope is used to monitor the surface in between polishing steps and adjust the polishing procedure, that is, corotational velocity of sample and polishing plate, pressure and duration.

Characterization methods

Several microscopic techniques are applied to demonstrate features of the RDX crystal defects. Using an optical microscope in incident light reflection mode, voids in the crystals are clearly demonstrated. Differential interference contrast shows small surface features at the cross-sections. Both characterizations are carried out with a Leica LM optical microscope. More details at the surface of the cross-section can be observed by a FEI NovaNanoSEM 650 scanning electron microscope. The microscope is operated in 100 Pa low-vacuum mode to avoid electrical charging and sublimation in high vacuum. Typical

operating conditions are 4–6-kV acceleration voltage and a 6–8-mm working distance. A Leica TCS SL confocal system with a DM6000 B microscope is used to obtain the CSLM images. In reflection mode, the optical slices have a thickness down to about 0.5 μm . Local differences in refractive index inside the RDX crystal are revealed as bright spots against a dark background. The original CSLM images are inverted by image processing, showing grey/black spots against a white background, since this provides a better contrast.

Results and discussion

Optical microscopy

The origin of the observed defects is most likely related to the crystal growth process of the RDX during its production. Only general remarks can be made on the formation of defects and their relation to the crystallization process, because detailed information on the crystallization and process conditions during the production of the different RDX batches is not available. Generally, during the growth of a crystal, the growth conditions, such as supersaturation, impurity concentration and boundary layer thickness, may vary locally. These variations are reflected in single crystals in the form of growth banding, growth sectors and sector boundaries. These may introduce dislocations, inclusions, the uptake of impurities and other lattice defects in the growing crystal. Such inclusions are visible in the optical micrographs of Figures 1–3, which are made in incident light reflection mode. Typical dimensions of the inclusions are 10–40 μm in K1 and K6 and only up to

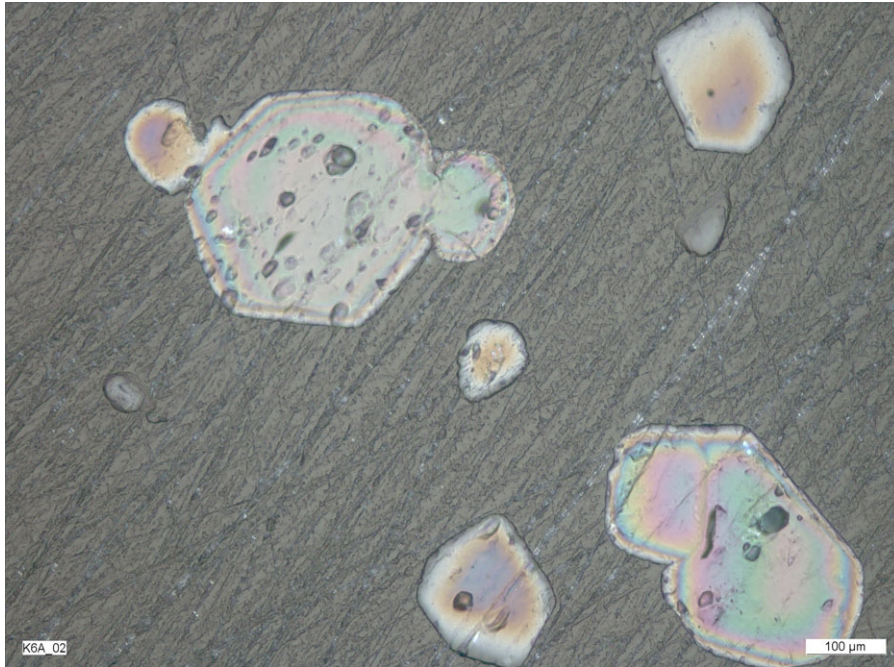


Fig. 2. Optical micrograph of K6 RDX crystals in incident light mode.

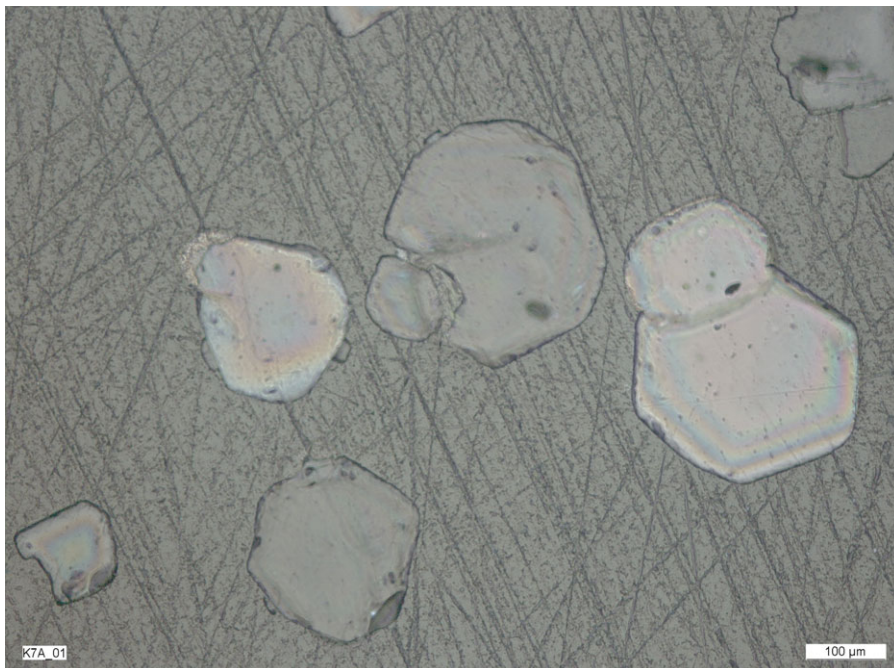


Fig. 3. Optical micrograph of K7 RDX crystals in incident light mode.

a few micrometres in K7. Growth bands and growth sectors are observed in K6 and K7, but not in K1, when observing dissections of these crystals by means of differential interference contrast microscopy (DICM), see Figures 4–6. This technique uses interference of two orthogonally polarized light beams which increases the contrast due to optical path differences. In Figure 6, two parallel defect planes, not being polishing de-

fects, are visible about 150-μm apart from each other. These defects seem to be correlated with one specific crystallographic orientation. Each growth band and growth sector has a specific crystallographic orientation of the RDX molecular structure. It appears that the defect itself can cross multiple growth sectors, but the crystallographic structure is maintained across these sectors.

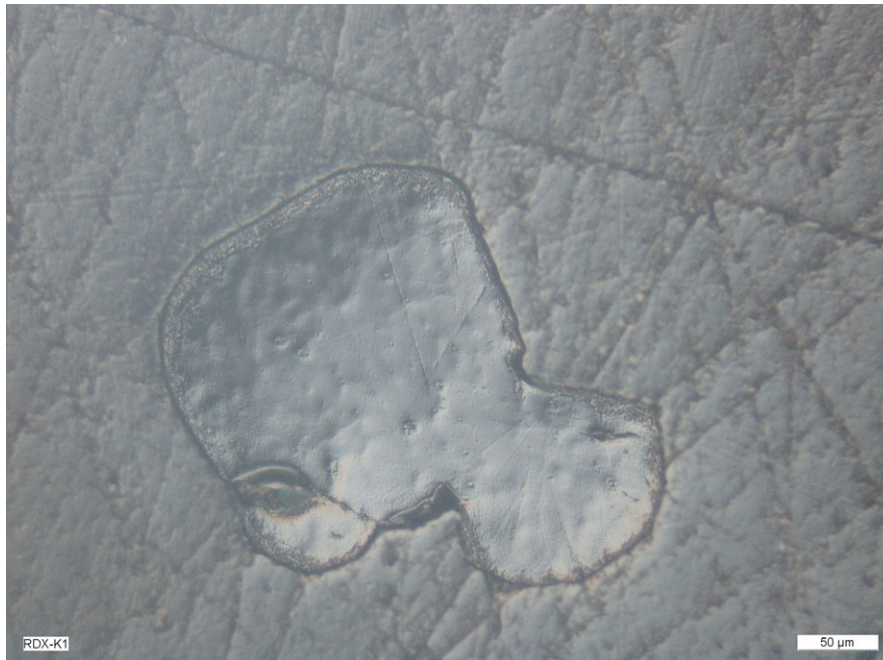


Fig. 4. Optical micrograph of K1 RDX crystal in differential interference contrast mode.



Fig. 5. Optical micrograph of K6 RDX crystal in differential interference contrast mode.

SEM

Typical scanning electron micrographs for K1 crystals are shown in Figures 7–9. The large spherical or ellipsoidal voids with smooth internal surface in Figure 7 originate from air and solvent inclusions. Occasionally, areas with submicron voids

are found, see Figure 8. At the interface of grains, no irregularities are observed. Large epoxy-filled cavities like in Figure 9 can be present in K1 crystals. These pockets were accessible by the epoxy during sample preparation. These internal cavities in K1 crystals were not noticed before in scanning electron micrographs as no cross-sectioning procedure was applied (Watt



Fig. 6. Optical micrograph of K7 RDX crystal in differential interference contrast mode.

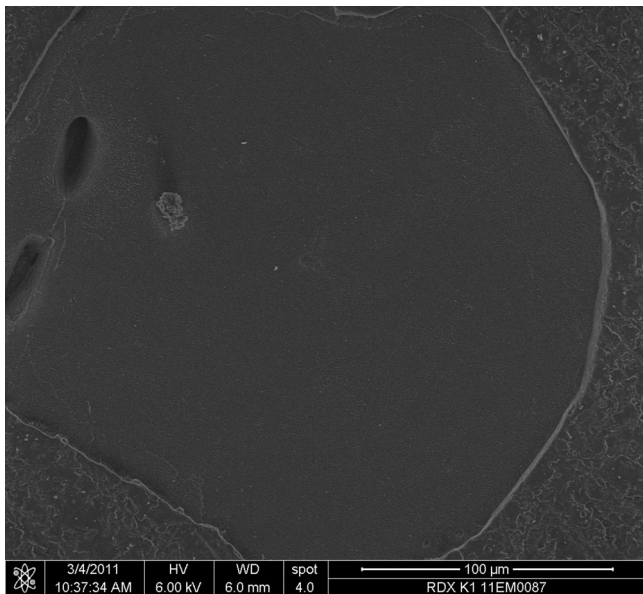


Fig. 7. Scanning electron micrograph of K1 RDX crystal.

et al., 2006). The filling of such a cavity in a crystal during the casting of a PBX might be difficult and, in the worst case, leave a void, which can act as a so-called hot spot in accidental shock impact scenarios (Van der Heijden & Bouma, 2004). Figure 10 is a single observation in the multitude of studied K1 crystals, showing a large void, with irregular steps and smooth surface. In contrast to cavities like in Figure 9, this defect was not filled with epoxy during sample preparation. The defect is either an

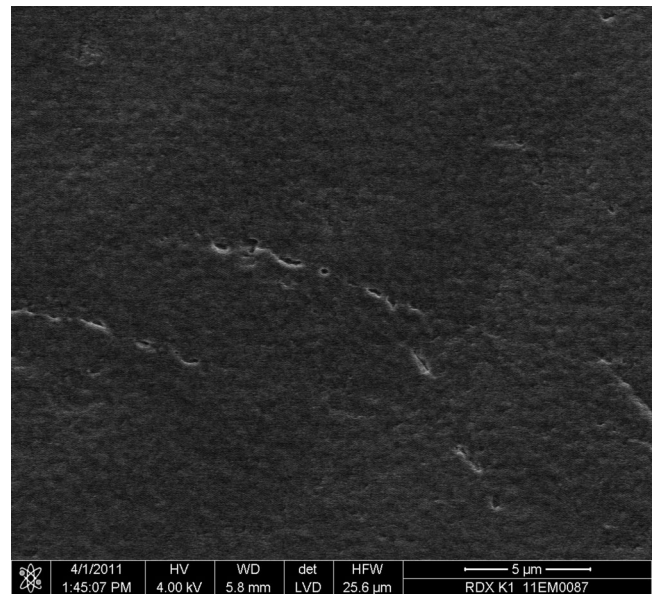


Fig. 8. Scanning electron micrograph of K1 RDX crystal.

inclusion or due to dislodging of an agglomerate in the sample preparation.

In many of the K6 crystals that were examined, a large number of submicron voids can be observed throughout a crystal cross-section, see Figures 11 and 12. These submicron voids, as observed before in a single crystal, cleaved with a scalpel (Bouma *et al.*, 2008; Van der Heijden *et al.*, 2008) are thus typical for this entire production lot. Submicron inclusions

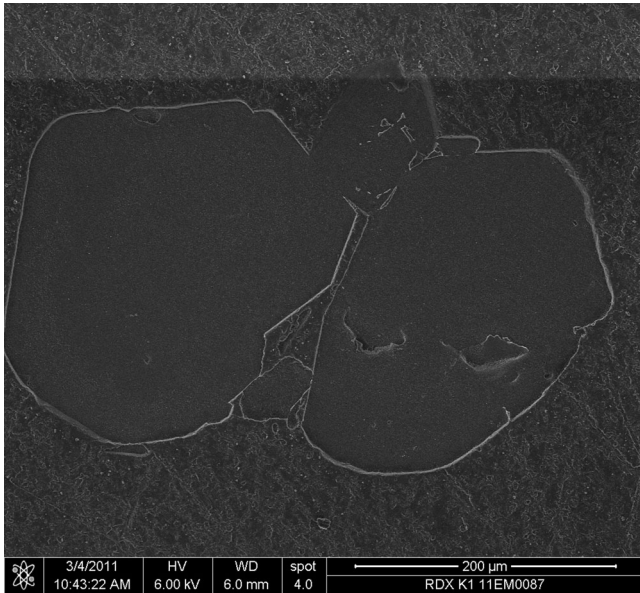


Fig. 9. Scanning electron micrograph of K1 RDX crystal.

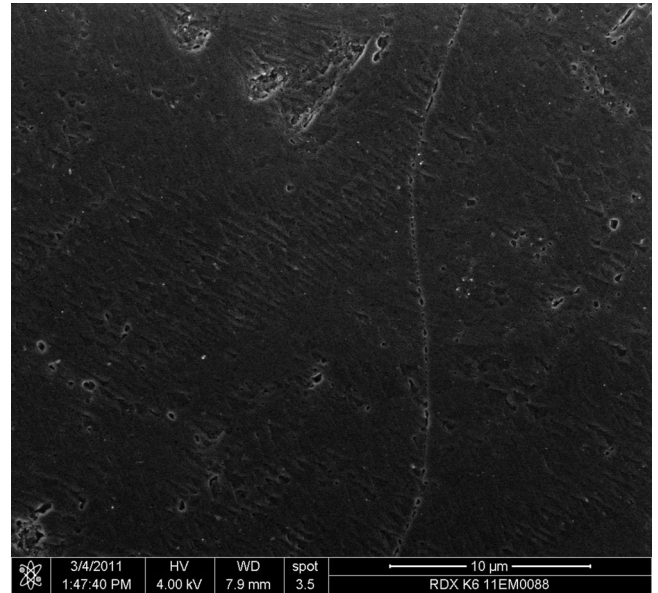


Fig. 11. Scanning electron micrograph of K6 RDX crystal.

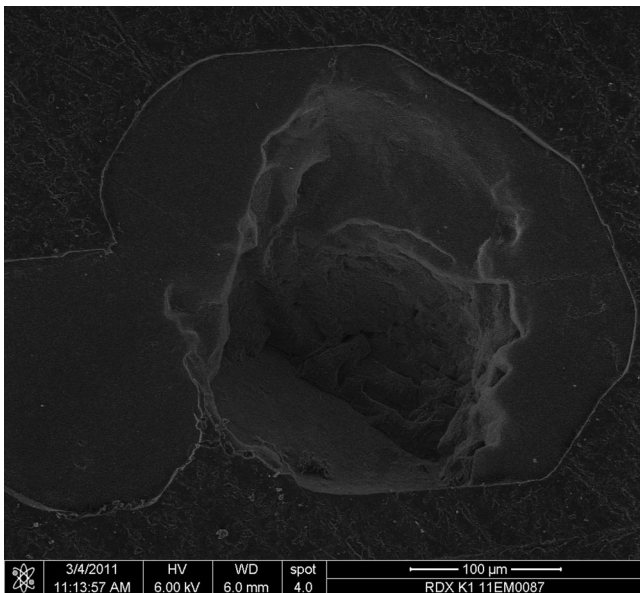


Fig. 10. Scanning electron micrograph of K1 RDX crystal.

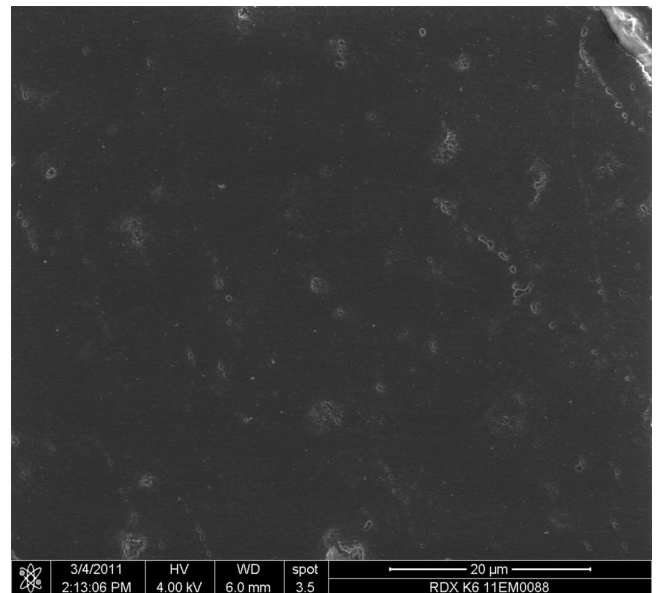


Fig. 12. Scanning electron micrograph of K6 RDX crystal.

aligned as a 'pearl necklace' are identified, see Figure 11. Grains can merge without entrapped volume, as shown in Figure 13. This image also shows a relatively large elongated void, with dimensions of $\sim 15 \times \sim 40 \mu\text{m}$.

Spherical and ellipsoidal voids typical for air and/or solvent inclusions are found in the K7 crystals, see Figure 14. Typical for the K7 crystals are sharp-edged and almost crack-like defects across the entire single crystal. In many cases multiple and parallel planar defects are observed, about $10 \mu\text{m}$ or even more than $100\text{-}\mu\text{m}$ apart, see Figures 15 and 16, respectively. It indicates a preferential crystallographic orientation at which

these defects emerge. Another typical feature of the K7 crystals are those locations where several grains have grown towards each other, and where a void with an irregular cross-section remains, see Figure 17.

Figure 11 also shows regular features, which appeared when observing RDX samples again after they had been in the SEM under ultrahigh vacuum for several days. The appearance of features at the surface of RDX, limits the duration one can keep RDX samples (relatively) unchanged at high vacuum and/or reduced pressures as are generally applied in a SEM. These new surface features show similarities with the etch pits

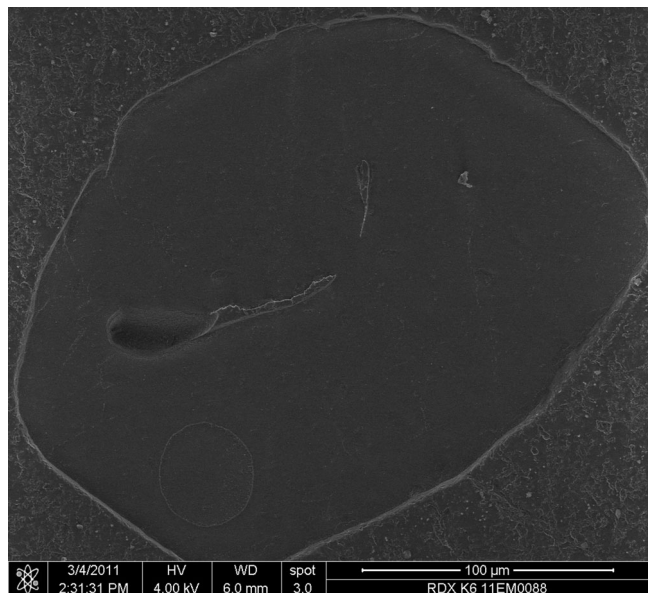


Fig. 13. Scanning electron micrograph of K6 RDX crystal.

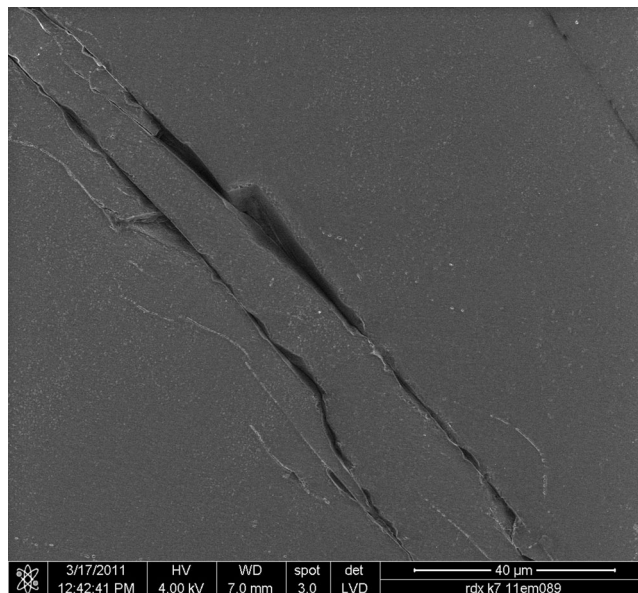


Fig. 15. Scanning electron micrograph of K7 RDX crystal.

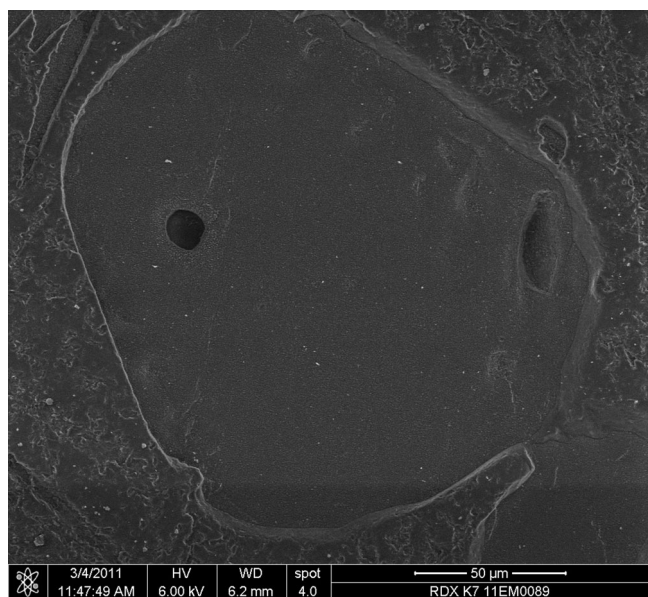


Fig. 14. Scanning electron micrograph of K7 RDX crystal.

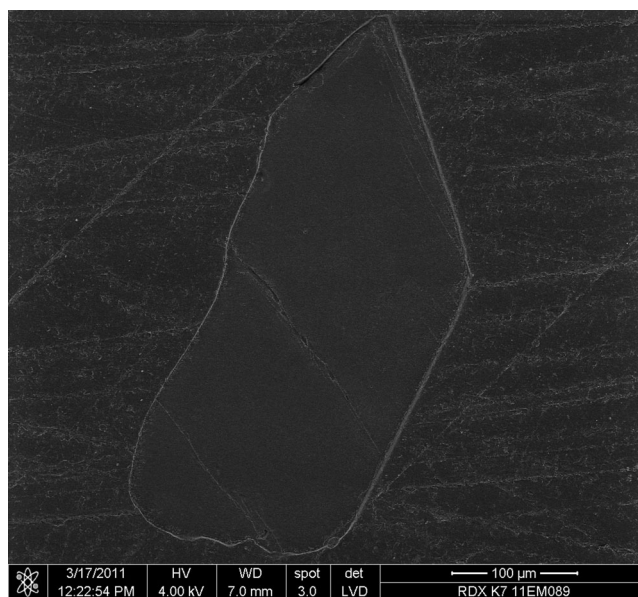


Fig. 16. Scanning electron micrograph of K7 RDX crystal.

as observed, for example, by Armstrong & Elban (2004) after slight dissolution of specific RDX crystal faces. Based on these similarities, it is assumed that the regular features shown in Figure 11 can be attributed to 'etching' effects. It is known that etch pits are formed due to preferential dissolution of dislocation lines emerging at the surface of a crystal. The preferential dissolution is related to areas of mechanical stress localized at and around the dislocation line, which leads to a higher dissolution rate compared to that of nonstressed areas (Van der Hoek *et al.*, 1982; Van der Heijden & Van der Eerden, 1992). The morphology of the etch pits generally follows the (point

group) symmetry depending on the crystallographic orientation of the crystal face on which the etch pits have been formed (Van der Heijden & Geertman, 1992). Since the orientation of the RDX crystals embedded in the epoxy is random, the crystallographic orientation of the polished RDX surfaces differs from crystal to crystal and therefore also the morphology of the pits as a result of the etching effect may differ from one particle to another. However, the fact that the pits, shown in Figure 11, all have the same orientation and direction is an indication that these pits have been formed along dislocation lines. Because the etch effects appear only when storing the

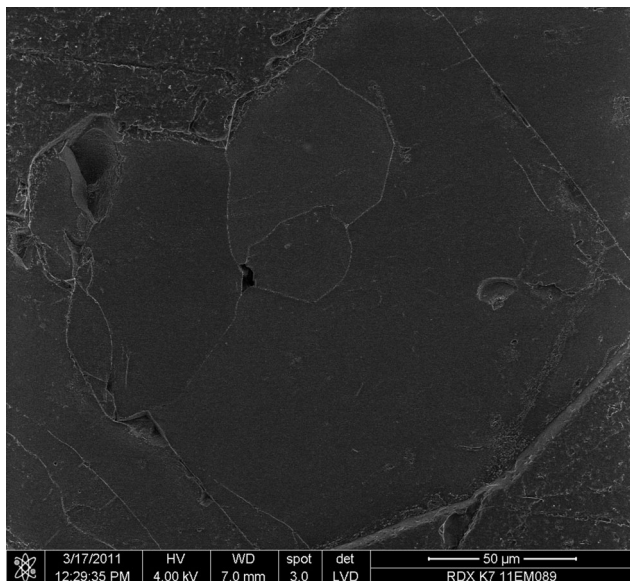


Fig. 17. Scanning electron micrograph of K7 RDX crystal.

samples under ultrahigh vacuum, the etching is very likely due to sublimation of RDX from the RDX surfaces exposed to the vacuum. In order to judge whether sublimation can be an explanation of the formed etch pits, an estimate was made of the amount of sublimed material from an RDX crystal surface of $100 \times 100 \mu\text{m}^2$. Gershanik & Zeiri (2012) measured the sublimation rate of RDX in air for temperatures of 60°C , 65°C and 70°C . Assuming an Arrhenius-type dependence of sublimation rate on temperature, an activation energy of 114 kJ mole^{-1} has been determined by Gershanik & Zeiri (2012). By extrapolation to room temperature, a sublimation rate of 0.23 ng h^{-1} can be calculated. For a 3 days storage of the RDX samples in ultrahigh vacuum, this leads to a total mass of sublimed RDX of 17 ng. For an area of $100 \times 100 \mu\text{m}^2$, this corresponds to a sublimation of a layer of $\sim 1\text{-}\mu\text{m}$ thickness (density of RDX is 1.82 g cm^{-3} , thickness of one molecular layer $\sim 1 \text{ nm}$; this latter value is an approximate value based on the lattice constants of the orthorhombic crystal structure of RDX: $a = 13.182$, $b = 11.574$ and $c = 10.709 \text{ \AA}$; Herrmann & Fietzek, 2005). The estimated value for the sublimed layer thickness of $\sim 1 \mu\text{m}$ appears to be in the same range as the surface features that can be observed in Figure 11, indicating that sublimation of the RDX in ultrahigh vacuum can be a realistic explanation. It should be realized that the estimated value for the sublimed layer thickness is probably only a lower limit, since its estimation is based on sublimation rate data in air, whereas it can be assumed that under ultrahigh vacuum conditions the sublimation rate will be higher than at ambient pressure.

CSLM

Typical CSLM images of K1, K6 and K7 crystals are shown in Figure 18–20, respectively. The original images show bright



Fig. 18. Inverted confocal scanning laser micrograph ($375 \times 375 \mu\text{m}$) of K1 RDX crystal.

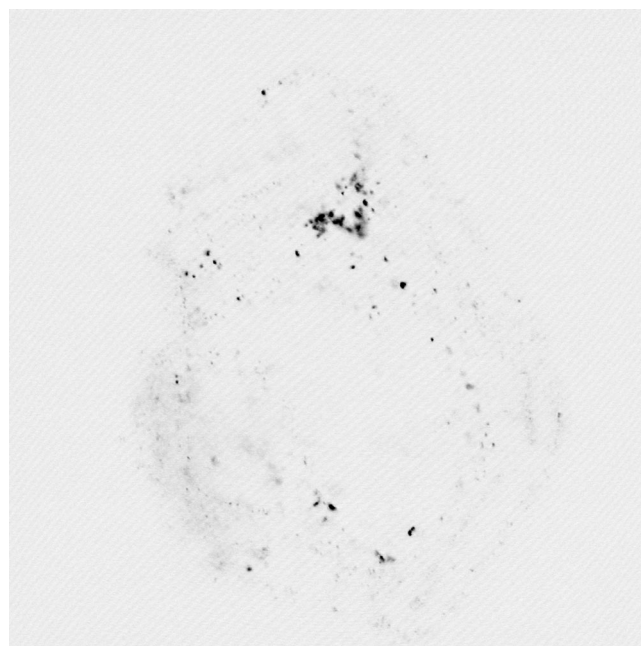


Fig. 19. Inverted confocal scanning laser micrograph ($93.5 \times 93.5 \mu\text{m}$) of K6 RDX crystal.

spots against a dark background as a result of differences in refractive index, most likely caused by inclusions or voids present in the crystal. The K1 crystals do contain a few inclusions/voids. More inclusions are observed in K6 and K7. In K6 and specifically in K7 crystals, the inclusions appear to be mainly localized in the periphery of the crystals, whereas the

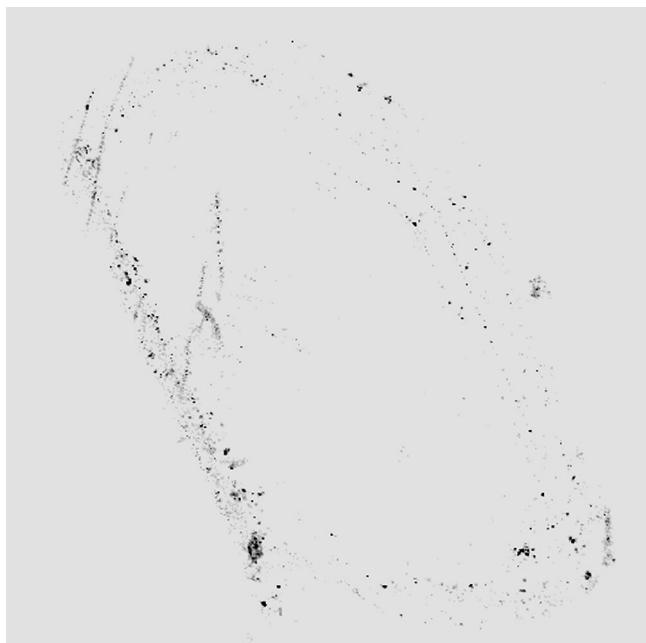


Fig. 20. Inverted confocal scanning laser micrograph ($375 \times 375 \mu\text{m}$) of K7 RDX crystal.

central part is relatively 'clean'. The spots in the CSLM images of K6 crystals appear to be more 'blurred' compared to those in the other two RDX batches. This can point at the presence of regions with a higher (mechanical) stress, leading to a different refractive index of that specific area. In subsequent CSLM slices, approximately $0.5\text{-}\mu\text{m}$ apart, generally different spots are visible at different locations, which indicates that at least a number of the inclusions is in the order of $0.5 \mu\text{m}$ or smaller. The findings shown in Figures 8, 11 and 12 are in line with SEM observations on cleaved crystal surfaces (Bouma *et al.*, 2008; Van der Heijden *et al.*, 2008), as well as with earlier CSLM observations using different product qualities of HMX crystals (Van der Heijden & Bouma, 2004).

The RDX crystals that have been examined by means of optical microscopy, SEM and CSLM, each represent different samples obtained from the original RDX batches. In the order of a few hundreds of crystals are available at the polished sample surface. Optical microscopy is used to verify crystal features in a large multitude of crystals. For SEM and CSLM, generally about five to ten crystals have been examined in more detail, and a selection of those images displaying the typical features observed in these crystals has been included in this paper. The RDX batches examined in this study have been the subject of previous characterization studies, including optical microscopy and SEM (Doherty & Watt, 2008; Van der Heijden *et al.*, 2008; Van der Heijden & Bouma, 2010; Hudson *et al.*, 2013), and comparison of the current observations with those reported in the other characterization studies shows similar results for the different RDX batches investigated here.

Table 2. Summary of defects (macro-, microinclusions, intragranular voids, cracks) and observations (growth bands and sectors) with optical, scanning electron and confocal scanning laser microscopy

Defects and observations	K1	K6	K7
Macroinclusions	Yes	Yes, many	Hardly
Microinclusions	Yes, few	Yes, many ^a	Yes
Intragranular voids	No	No	Yes
Cracks	No	No	Yes
Growth bands	No	Yes	Yes
Growth sectors	No	Yes	Yes

^aIncluding micro-inclusions aligned as a 'pearl necklace'.

This provides confidence that the samples are representative of the larger batches. The current sample preparation allows for the analysis of many crystals regardless of their size, in contrast to the previously reported manual cleaving of a single and relatively large crystal for SEM analysis (Van der Heijden *et al.*, 2008).

Both the optical microscopy and SEM images represent 2D imaging techniques. Although also the CSLM technique records 2D slices, it can be considered a 3D imaging technique: by displaying subsequently recorded 2D slices one after the other, one in fact moves through a 3D part of the crystal. This evidently is an advantage compared to the other two imaging techniques, since it provides information on how the defects extend not only in 2D (lateral) but also in 3D.

The variety in defects in the three RDX grades as observed by the different microscopic techniques, is summarized in Table 2. It is well known that voids and inclusions become hot spots when interacting with a shock wave. For a shock to develop into a detonation, it is generally assumed that the void size cannot be below $0.1 \mu\text{m}$, as the local decomposition would quench too quickly to produce ignition (Field, 1992). Numerical modelling of the hot spot behaviour with hot spots at periodic intervals, studying how the reaction waves, propagating from multiple hot spots, would interact at mesoscale was carried out by Handley (2011). Numerical results for HMX indicated a critical hot spot size between 0.5 and $0.25 \mu\text{m}$. Recently, both heterogeneous and homogeneous ignition behaviour were demonstrated in the shock initiation of mixtures of nitromethane and silica beads of $1\text{--}4 \mu\text{m}$ and $40 \mu\text{m}$, with the smaller beads being more sensitizing than the larger beads (Dattelbaum *et al.*, 2010). Furthermore, the authors mentioned that also the number density of hot spots plays a role in sensitizing mixtures of nitromethane and silica beads.

Extrapolating the conclusions of Handley (2011) and Dattelbaum *et al.* (2010) to this study, single voids and defects in the range of $0.5\text{--}10 \mu\text{m}$, like those observed in this investigation, are expected to be important parameters determining the shock initiation of the PBXN-109 compositions with different qualities of RDX. Referring to the work of Dattelbaum *et al.* (2010), the presence of a submicron void may not be

decisive in sustaining a reactive wave; it might be the difference in number density of (sub)micron voids in K1 and K6 crystals that makes the PBXN-109 containing the K6 grade more susceptible to shock initiation than the one containing the K1 crystals.

The details obtained on the defects present in the examined RDX crystals can be used to further refine the modelling of energetic composite materials. Lately, significant steps forward have been achieved in describing the heterogeneity of energetic composite materials like PBXs, for example, by developing algorithms to create polydisperse packs of nonspherical shapes of granular explosives (Stafford & Jackson, 2010), by including the effect of metal particles on the deformation-induced heating of an explosive composite (Chakravarthy *et al.*, 2013) and by modelling the hot-spot formation in granular and in PBXs (Handley, 2011; Barua *et al.*, 2013). In the hot-spot modelling, mechanical loading of energetic composites cause frictional dissipation as a result of grain fracture or due to interparticle contacts, leading to local temperature increases that act as hot spots. Based on the current results, modellers are encouraged to extend and refine their models to include typical defects (size, type and quantity) as described in this paper for RDX, and to elucidate how these defects, when interacting with a shock wave, affect the local temperature fields, particularly in the interior of the energetic particles.

Conclusions

Three batches of the commercial energetic material RDX, referred to as K1, K6 and K7, differing in shock sensitivity, have been characterized with different microscopic techniques in order to visualize the defect content in these crystals.

Optical microscopy in incident light reflection mode on crystals that were embedded in an epoxy resin and then cut and polished reveals internal voids and inclusions in the crystals for all of the three batches. By using DICM, growth bands and growth sectors have been observed in K6 and K7 crystals, as well as defects that are aligned with the crystallographic structure.

A comparison between scanning electron micrographs of random cross-sections in a multitude of crystals and micrographs of single crystals that have been cleaved to obtain fracture along a defect-rich plane has revealed the existence of different types of defects, which were found to be specific for each source of the RDX batches. Furthermore, the existence of sub-micron voids has been demonstrated. This was also confirmed by CSLM characterization of the three RDX batches, revealing local differences in refractive index, pointing at inclusions or voids within the crystals. Inclusions as small as approximately 0.5 μm have been observed by using this method.

It is well known that voids and inclusions become hot spots when interacting with a shock wave. Single voids and 0.5–10- μm sized defects as well as the number density of the (sub)micron voids appear to play an important role in the

shock initiation of the PBXN-109 compositions with different qualities of RDX.

The obtained experimental results comprise details on the size, type and quantity of the defects. These details should provide modellers with relevant and realistic information for modelling defects in energetic materials and their effect on the initiation and propagation of shock waves in PBX formulations.

Acknowledgements

The authors acknowledge support from the U.S. Defense Threat Reduction Agency under project award HDTRA1-10-1-0078. Mrs A.M.A. van der Laan is acknowledged for assistance during the measurements with the confocal scanning laser microscope, department of Molecular Cell Biology at the Leiden University Medical Center (LUMC), the Netherlands. Dr C.A. van Driel is acknowledged for reviewing the manuscript.

References

- Armstrong, R.W. & Elban, W.L. (2004) *Dislocations in Energetic Crystals in Dislocations in Solids*, Vol. 12 (ed. by F.R.N. Nabarro and J.P. Hirth). Elsevier Science Publishers, the Netherlands.
- Baer, M.R. (2002) Modeling heterogeneous energetic materials at the mesoscale. *Thermochim. Acta*, **384**, 351–367.
- Barua, A., Kim, S., Horie, Y. & Zhou, M. (2013) Ignition criterion for heterogeneous energetic materials based on hotspot size-temperature threshold. *J. Appl. Phys.*, **113**, 064906.
- Beauregard, R.L. (2004) History of the U.S. Navy Insensitive Munitions Program.
- Borne, L. (1993) Influence of intragranular cavities of RDX particle batches on the sensitivity of cast wax bonded explosives. In *Proceedings of the 5th Congrès International de Pyrotechnie*, EUROPYRO 93, Strasbourg, France, p. 155.
- Bouma, R.H.B., Boluijt, A.G., Verbeek, H.J. & Van der Heijden, A.E.D.M. (2008) On the impact testing of cyclotrimethylene trinitramine crystals with different internal qualities. *J. Appl. Phys.*, **103**, 093517.
- Chakravarthy, S., Gonthier, K.A. & Panchadhara, R. (2013) Analysis of mesoscale heating by piston supported waves in granular metalized explosive. *Modelling Simul. Mater. Sci. Eng.*, **21**, 055016.
- Dattelbaum, D.M., Sheffield, S.A., Stahl, D.B., Dattelbaum, A.M., Trott, W. & Engelke, R. (2010) Influence of hot spot features on the initiation characteristics of heterogeneous nitromethane. In *Proceedings of 14th International Detonation Symposium*, Office of Naval Research.
- Doherty, R.M., Watt, D.S. & Nock, L. (2006) Reduced sensitivity RDX round robin program. In *Proceedings of Insensitive Munitions and Energetic Materials Technology Symposium*, Bristol.
- Doherty, R.M. & Watt, D.S. (2008) Relationship between RDX properties and sensitivity *Propell. Explos. Pyrotech.*, **33**, 4–13.
- Field, J.E. (1992) Hot spot ignition mechanisms for explosives. *Acc. Chem. Res.*, **25**, 489–496.
- Field, J.E., Bourne, N.K., Palmer, S.J.P., Walley, S.M., Sharma, J. & Beard, B.C. (1992) Hot-Spot Ignition Mechanisms for Explosives and Propellants [and Discussion]. *Philos. Trans. R. Soc. Lond. A Biol. Sci.*, **339**, 269–283.
- Förster-Barth, U., Herrmann, M., Mathieu, J., & Patscheider, J. (2007) Investigation of RS-RDX samples from the MSIAC-Round robin by means

- of X-ray diffraction rocking curves. In *Proceedings of the 39th International Annual Conference of ICT*, Karlsruhe.
- Freche, A., Aviles, J., Donnio, L., & Spyckerelle, C. (2000) Insensitive RDX (I-RDX). In *Proceedings of Insensitive Munitions and Energetic Materials Symposium*, San Antonio.
- Gershanik, A.P. & Zeiri, Y. (2012) Sublimation rate of energetic materials in air: RDX and PETN. *Propell. Explos. Pyrotech.*, **37**, 207–214.
- Handley, C.A. (2011) *Numerical modelling of two HMX-based plastic-bonded explosives at the mesoscale*. PhD Thesis, University of St Andrews, UK.
- Herrmann, M. & Fietzek, H. (2005), Investigation of the microstructure of energetic crystal by means of X-ray powder diffraction, JCPDS—International Centre for Diffraction Data, *Advances in X-ray Analysis*, Volume **48**.
- Hudson, R., Zioupos, P. & Gill, P.P. (2013), Investigating the mechanical properties of RDX crystals using nano-indentation. *Propell. Explos. Pyrotech.*, **37**, 191–197.
- Kröber, H., Teipel, U., Leisinger, K. & Krause, H. (1998), Formation of HMX-crystals with high internal quality by cooling crystallization. In *Proceedings of the 29th International Annual Conference of ICT*, pp. 66–1–66–18. Karlsruhe, Germany.
- Moulard, H. (1989), Particular aspect of the explosive particle size effect on shock sensitivity of cast PBX formulations. In *Proceedings of the 9th Symposium (International) on Detonation*, Portland, USA.
- Qiu, H., Stepanov, V., Di Stasio, A.R., Chou, T. & Lee, W.Y. (2011) RDX-based nanocomposite microparticles for significantly reduced shock sensitivity. *J. Hazard. Mater.*, **185**, 489–493.
- Spyckerelle, C. (2006) Minutes of the RS-RDX Round Robin (R4), *Technical Meeting*, NATO-MSIAC report L-130.
- Spyckerelle, C., Eck, G. & Guillaumin, J. (2010) Method for determining the sensitive or insensitive nature of a hexogen. US Patent 2010/0258223 A1.
- Stafford, D.S. & Jackson, T.L. (2010) Using level sets for creating virtual random packs of non-spherical convex shapes. *J. Comput. Phys.*, **229**, 3295–3315.
- Van der Heijden, A.E.D.M. & Bouma, R.H.B. (1998), Shock sensitivity of HMX/HTPB PBX's: relation with HMX crystal density. In *Proceedings of the 29th International Annual Conference of ICT*, Karlsruhe, Germany.
- Van der Heijden, A.E.D.M. & Bouma, R.H.B. (2004) Crystallization and characterization of RDX, HMX and CL-20. *Cryst. Growth Design*, **4**, 999–1007.
- Van der Heijden, A.E.D.M. & Bouma, R.H.B. (2010) Energetic materials: crystallization and characterization. *Handbook of Material Science Research* (ed. by C. René and E. Turcotte), p. 323, Nova Science Publishers, Hauppauge, NY.
- Van der Heijden, A.E.D.M., Bouma, R.H.B. & Van der Steen, A.C. (2004) Physicochemical parameters of nitramines determining shock sensitivity. *Propell. Explos. Pyrotech.*, **29**, 304–313.
- Van der Heijden, A.E.D.M., Bouma, R.H.B. & Van Esveld, R.J. (2000), Shock sensitivity of HMX based compositions. In *Proceedings of the 31st International Annual Conference of ICT*, Karlsruhe, Germany.
- Van der Heijden, A.E.D.M., Creighton, Y.L.M., Marino, E., Bouma, R.H.B., Scholtes, J.H.G., Duvalois, W. & Roelands, C.P.M. (2008) Energetic Materials: crystallization, characterization and insensitive plastic bonded explosives. *Propell. Explos. Pyrotech.*, **33**, 25.
- Van der Heijden, A.E.D.M. & Geertman, R.M. (1992) Etch pits on caprolactam. *J. Crystal Growth*, **123**, 321.
- Van der Heijden, A.E.D.M. & Ter Horst, J.P. (2005) Crystallization and product quality. *Energetic Materials—Particle Processing and Characterization* (ed. by U. Teipel), ISBN 3–527–30240–9, 2005, Wiley-VCH, Germany.
- Van der Heijden, A.E.D.M. & Van der Eerden, J.P. (1992) Growth rate dispersion: the role of lattice strain. *J. Crystal Growth*, **118**, 14–26.
- Van der Hoek, B., Van der Eerden, J.P. & Bennema, P. (1982) Thermodynamical stability conditions for the occurrence of hollow cores caused by stress of line and planar defects. *J. Crystal Growth*, **56**, 621–632.
- Watt, D.S., Doherty, R.M. & Nock, L. (2006) RS-RDX Round Robin (R4) Preliminary Results Analysis, NATO-MSIAC report L-127.